Theoretical investigation of the effect of asymmetry on optical anisotropy and electronic structure of Stranski-Krastanov quantum dots

Jitendra Kumar, Sheetal Kapoor, Saral K. Gupta, and Pranay K. Sen*
Department of Applied Physics, Shri G. S. Institute of Technology and Science, 23 Park Road, Indore-452003, India
(Received 17 March 2006; revised manuscript received 3 August 2006; published 26 September 2006)

The effect of size and shape anisotropy on the optical properties of Stranski-Krastanov quantum dots (QDs) is theoretically investigated. The QD is modeled using anisotropic parabolic confinement potential. The complex structure of the valence band is described by Luttinger Hamiltonian. The energy spectra and eigenfunctions of hole states are calculated by numerical diagonalization of the Hamiltonian. The dipole matrix elements are obtained for the interband transitions and hence the degree of linear polarization is calculated. The formulation is applied to self-assembled CdSe quantum dots for numerical analysis. The variation of energy eigenvalues with the QD shape anisotropy parameter is studied and the effect of valence subband mixing is clearly identified. The crossings and anticrossings of the valence subbands have been explained in terms of the symmetries of the corresponding eigenstates. It is worthy to note that these symmetry properties of the energy states are responsible for the specific types of dipole selection rules for the anisotropic QDs. The degree of linear polarization is found to increase almost linearly with anisotropy parameter for the transitions from heavy-hole ground states. On the contrary, for the excited hole states, the change is nonmonotonic due to strong anisotropy-dependent mixing effects.

DOI: 10.1103/PhysRevB.74.115326 PACS number(s): 78.67.Hc, 73.21.La, 78.55.Et

I. INTRODUCTION

Semiconductor quantum dots (QDs) exhibit electronic and optical properties quite different from those of the bulk semiconductors, as the quantization of all degrees of freedom results in atomlike discrete set of energy levels. The electronic structure of the QD can be manipulated by varying the shape, size, and number of electrons associated with it. Size and shape anisotropies play key roles in determining the transition energies in a QD and strongly influences its optical response. In contrast to nonpolarized radiation arising from spherical QDs, anisotropic dots give rise to radiation that is strongly linearly polarized.[1]

In recent years, great progress has been made in the fabrication of semiconductor QDs especially those grown by Stranski-Krastanov (SK) technique.[2–7] In this technique, material is deposited epitaxially onto a substrate to which it is not lattice matched. Due to the mismatch, the deposited material spontaneously forms nanometer scale islands. Material parameters and the growth conditions decide the size and shape of these self-assembled QDs. It is observed that there can be significant in-plane anisotropy in the growth of SK QDs.[8–10] This anisotropy can alter the electronic properties of the QDs and lift the degeneracy of the different excited hole states.

The optical properties of self-assembled QDs have been studied experimentally extensively using various techniques. Photoluminescence (PL) spectrum is an efficient tool to gain information about the symmetry of emission states and relaxation processes of excited carriers. The polarization state of the emitted light depends on the symmetry of the wave function and thus provides indirect information about the geometric symmetries of the QDs.[1] In this context, polarization-resolved photoluminescence experiments have attracted much attention in the recent past. Experimental evidence of pronounced optical anisotropy has been reported for various QD systems including InAs/GaAs QDs[11] and CdSe/ZnSe QDs.[9,10,12,13]

High degree of polarizaton of PL spectra can be associated with the QD shape and anisotropic strain distribution.[7,8,14,15] Detailed investigation of the effect of anisotropy and Coulomb interaction on the electronic structure of two-electron QDs has revealed complex spectral properties resulting from various configurations of the confinement.[16] Finley *et al.*[17] have observed that the PL spectra of InAs QDs consist of linearly polarized doublet arising due to the anisotropic exchange interaction, though, clear identification of the roles played by enhanced confinement and the shape anisotropy have not been made. In case of the negatively charged excitons known as trions, the total spin of the two electrons is zero in the spin singlet ground state, the electron-hole (e-h) exchange interaction vanishes and the polarization anisotropy is determined solely by the light-hole (lh) and heavy-hole (hh) mixing.[12] The fine structure of the excitonic levels is determined by a combination of lh-hh mixing and e-h exchange interactions. Typically, for CdSe/ZnSe QDs the exchange splitting is as small as 0–0.5 meV.[9] The coupling energy can be an order of magnitude larger than the exchange energy, if the lh-hh levels are reasonably close. This is also supported by the experimental results of Favero *et al.*[18] where the fine structure splitting is not observable for their QD sample showing large degree of polarization. Thus, lh-hh coupling is the dominant mechanism for the quantum dots exhibiting pronounced optical anisotropy and the polarization arising due to exchange processes can be neglected without losing much degree of accuracy.

Research has been taken up by many well-known scientific groups world over, to formulate theoretical models and explain the results accurately, as obtained in a wide range of experiments pertaining to the optical properties of QDs. These models are based on different QD geometries and

forms of the confinement potential ranging over the spherical[19] or infinite wall cylindrically symmetric potentials,[20] lens geometry,[21–23] ellipsoidal confinement,[24] rectangular hard walled potential,[25] trapezoidal QDs,[26] and parabolic confinement potential.[27–29] The two-dimensional harmonic oscillator potential explains quite accurately the shell structure revealed by the spectroscopy experiments.[28,29] Thus, this parabolic potential model is most commonly used for obtaining the electronic properties of the QDs. The magnetic field effects can also be incorporated easily in this formalism.[30]

The deep confinement potential offered by wide gap II-VI semiconductors, like CdSe, provides a higher flexibility for band-gap engineering. The growth of high quality CdSe/ZnSe QDs using SK technique has stimulated further interest in these quantum structures. In addition, the CdSe/ZnSe material combination is interesting because the lattice mismatch of CdSe on ZnSe is practically identical to that of the widely studied InAs/GaAs system.[4,5] CdSe is known to stabilize in wurtzite structure or zinc-blende structure depending on the growth conditions.[31] Experimental observations indicate that at low temperatures, CdSe is stable in zinc-blende structure. However, it is observed that calculations based on both wurtzite and zinc-blende structures yield good agreements with experimental data on electronic structure.[32]

The anisotropic strain distribution affects the electronic and optical properties of the QDs. The dominant contribution to the anisotropy of the strain distribution is caused by the anisotropy of the QD shape when the symmetry of the QD shape is less than or equal to the symmetry of the crystal structure.[33] The effect of strain on the electronic structure is twofold. The hydrostatic strain just causes a constant shift between the electron energy level and all the hole levels. The shear strain for the [001]-oriented zinc-blende crystal adds only to the diagonal terms of the Luttinger Hamiltonian. Therefore, strain does not induce any extra spin mixing but adjusts the relative positions of the *hh* and *lh* energy levels.[6,34,35]

In the present paper, we carry out the calculations for hole eigenstates in an anisotropic quantum dot modeled using parabolic confinement potential. We consider the case of a CdSe/ZnSe QD with zinc-blende symmetry. SK QDs exhibit a well-defined quantization axis (z axis) represented by the growth direction. The optical anisotropy as observed in QDs can be due to either the noncubic crystalline structure or the nonspherical shape since the polarization of the emission radiation depends on the symmetry of the wave function. The present work addresses the question as to how the in-plane anisotropy is manifested in the optical properties of a single QD. The effect of in-plane anisotropy is incorporated through the anisotropy of the confinement potential while the strain effects are treated phenomenologically through the *lh-hh* offset parameters. We have studied theoretically, the degree of linear polarization for a range of shape anisotropies varying from a circular shaped to a wirelike QD. Variable and complex spectral features occur as a result of various configurations of the confinement manifested in the form of energy gaps, level clustering, accidental degeneracies on one hand and level repulsions and avoided crossings, on the other. An important role is played by the mixing of *hh* and *lh* subbands in the quantum wells,[36] wires[37] as well as dots[27,38] which is apparent in the curves for the degree of linear polarization. This complex valence band structure has been incorporated in our calculations using the Luttinger Hamiltonian formalism.[39] We have numerically diagonalized the hole Hamiltonian over a wide range of both size and shape of the QDs, and clearly identified the effect of anisotropy and band mixing on the states. Further, we have calculated the degree of linear polarization of the photoluminescence for these anisotropic QDs, and established that shape and size variations of the QDs via band mixing effects can give rise to giant optical anisotropy.

The next two sections viz., Secs. II and III contain the details of the theoretical formulations of the model while the numerical analysis is presented in Sec. IV. Important conclusions have been drawn in Sec. V.

II. HAMILTONIAN FORMULATION

In the present work, we have considered a 4×4 Luttinger Hamiltonian for describing the valence band, while the conduction band is treated separately. We choose the z direction to be the crystal growth direction [001] for the CdSe QD with elliptical cross section in the (x-y) plane.

The wave functions in the envelope function approximation for the conduction band can be written as

$$\psi^c_{m_s}(\mathbf{r}) = f^c(\mathbf{r})u^c_{m_s}(\mathbf{r}), \tag{1}$$

where $u^c_{m_s}(\mathbf{r})$ are the two spin degenerate $\left(s=\frac{1}{2}, m_s=\pm\frac{1}{2}\right)$ bulk Bloch functions at the bottom of the conduction band, and $f^c(\mathbf{r})$ are the envelope functions. In the valence band, we have two spin degenerate *hh* and *lh* states, and the corresponding wave function is given by[40]

$$\psi^v(\mathbf{r}) = \sum_{m_j} f^v(\mathbf{r})u^v_{m_j}(\mathbf{r}). \tag{2}$$

Here, $u^v_{m_j}$ are the Bloch functions at the top of the valence band with $m_j=\pm\frac{3}{2}$ for the *hh* and $m_j=\pm\frac{1}{2}$ for the *lh* states corresponding to $j=\frac{3}{2}$. We have neglected the contribution from $j=\frac{1}{2}$ states as they are energetically well separated from $j=\frac{3}{2}$ states.

The Bloch wave functions for these energy states can be written as[41]

$$\left|\tfrac{3}{2},\tfrac{3}{2}\right\rangle = -\tfrac{1}{\sqrt{2}}(|x\uparrow\rangle + i|y\uparrow\rangle), \tag{3a}$$

$$\left|\tfrac{3}{2},\tfrac{1}{2}\right\rangle = -\tfrac{1}{\sqrt{6}}(|x\downarrow\rangle + i|y\downarrow\rangle) + \sqrt{\tfrac{2}{3}}|z\uparrow\rangle, \tag{3b}$$

$$\left|\tfrac{3}{2},-\tfrac{1}{2}\right\rangle = \tfrac{1}{\sqrt{6}}(|x\uparrow\rangle - i|y\uparrow\rangle) + \sqrt{\tfrac{2}{3}}|z\downarrow\rangle, \tag{3c}$$

and

$$\left|\tfrac{3}{2},-\tfrac{3}{2}\right\rangle = \tfrac{1}{\sqrt{2}}(|x\downarrow\rangle - i|y\downarrow\rangle). \tag{3d}$$

The envelope functions for the conduction band are obtained by solving the Schrödinger's equation with the parabolic confinement potential along the x-y plane, where the growth

direction is assumed to be along the z axis. The wave functions for the valence band can be obtained by solving the Luttinger Hamiltonian given by[39,40]

$$H = \begin{bmatrix} H_{hh} & c & b & 0 \\ c^\dagger & H_{lh} & 0 & -b \\ b^\dagger & 0 & H_{lh} & c \\ 0 & -b^\dagger & c^\dagger & H_{hh} \end{bmatrix} \begin{matrix} |3/2,3/2\rangle \\ |3/2,-1/2\rangle \\ |3/2,1/2\rangle \\ |3/2,-3/2\rangle. \end{matrix} \tag{4}$$

The individual matrix elements in Eq. (4) are given by

$$H_{hh} = -\frac{\hbar^2}{2m_0}\left[(\gamma_1 - 2\gamma_2)\frac{\partial^2}{\partial z^2} + (\gamma_1 + \gamma_2)\left(\frac{\partial^2}{\partial x^2} + \frac{\partial^2}{\partial y^2}\right) + V_z(z) + V_{xy}(x,y)\right], \tag{5a}$$

$$H_{lh} = -\frac{\hbar^2}{2m_0}\left[(\gamma_1 + 2\gamma_2)\frac{\partial^2}{\partial z^2} + (\gamma_1 - \gamma_2)\left(\frac{\partial^2}{\partial x^2} + \frac{\partial^2}{\partial y^2}\right) + V_z(z) + V_{xy}(x,y)\right], \tag{5b}$$

$$b = \frac{\sqrt{3}\hbar^2}{m_0}\gamma_2\frac{\partial}{\partial z}\left(\frac{\partial}{\partial x} - i\frac{\partial}{\partial y}\right), \tag{5c}$$

and

$$c = \frac{\sqrt{3}\hbar^2}{2m_0}\gamma_2\left(\frac{\partial}{\partial x} - i\frac{\partial}{\partial y}\right)^2. \tag{5d}$$

In the above equations, γ_1, γ_2, and γ_3 are the Luttinger parameters and we have considered the spherical approximation without sacrificing the accuracy. This approximation enables us to take $\gamma_2 \approx \gamma_3$ which removes the much involved band warping effects.[42] Moreover, this is consistent with the reported values of the Luttinger parameters for CdSe.[43–45] Further, it is expected that if shape anisotropy is significant, any small deviation from the above approximation would not lead to any substantial effect on the electronic structure.[46,47]

The in-plane confinement is defined by the anisotropic parabolic potential

$$V_{xy}(x,y) = \tfrac{1}{2}\alpha_x x^2 + \tfrac{1}{2}\alpha_y y^2. \tag{6}$$

The form of the confinement potential $V_z(z)$ along the z direction has not been assumed and the corresponding terms occurring in the analysis are to be treated as variable parameters of the QD structure. Without the off-diagonal terms the solutions (in x-y plane) would be the harmonic oscillator wave functions,

$$\phi_{n_x,lh}(x)\phi_{n_y,lh}(y), \quad \phi_{n_x,hh}(x)\phi_{n_y,hh}(y), \tag{7}$$

where n_x and n_y are the quantum numbers arising out of confinement along x and y directions, respectively. The form of these normalized wave functions is given by

$$\phi_{n_x,i}(x) = (2^{n_x} n_x! \sqrt{\pi}\lambda_{i,x})^{-1/2} \exp\left[-1/2\left(\frac{x}{\lambda_{i,x}}\right)^2\right] H_{n_x}\left(\frac{x}{\lambda_{i,x}}\right), \tag{8}$$

where

$$\lambda_{i,x} = \sqrt{\frac{\hbar}{m\omega_{i,x}}}, \tag{9}$$

and $i = lh, hh$.

Choosing the harmonic oscillator wave functions [Eq. (7)] as our basis, we can write down the matrix elements

$$H_{hh} = \left[E^z_{hh} + \hbar\omega^x_{hh}\left(n_x + \tfrac{1}{2}\right) + \hbar\omega^y_{hh}\left(n_y + \tfrac{1}{2}\right)\right]\delta_{n_x,n_x'}\delta_{n_y,n_y'}, \tag{10}$$

$$H_{lh} = \left[E^z_{lh} + \hbar\omega^x_{lh}\left(n_x + \tfrac{1}{2}\right) + \hbar\omega^y_{lh}\left(n_y + \tfrac{1}{2}\right)\right]\delta_{n_x,n_x'}\delta_{n_y,n_y'}, \tag{11}$$

where $\omega^x_{hh(lh)} = \sqrt{\alpha_x/m_{hh(lh)}}$ and $E^z_{hh(lh)}$ is the energy of $hh(lh)$ state due to z confinement.

It would be convenient to work in terms of the isotropic frequency ω_0 and the difference arising due to anisotropy as $\Delta\omega$. Thus we can write the hh and lh frequencies as

$$\omega^x_{hh} = (\omega_0 + \Delta\omega)\sqrt{\gamma_1 + \gamma_2}, \tag{12a}$$

$$\omega^y_{hh} = (\omega_0 - \Delta\omega)\sqrt{\gamma_1 + \gamma_2}, \tag{12b}$$

$$\omega^x_{lh} = (\omega_0 + \Delta\omega)\sqrt{\gamma_1 - \gamma_2}, \tag{12c}$$

$$\omega^y_{lh} = (\omega_0 - \Delta\omega)\sqrt{\gamma_1 - \gamma_2}. \tag{12d}$$

Anisotropy $\Delta\omega > 0$ means stronger confinement in the x direction while $\Delta\omega < 0$ means that the roles of x and y have been reversed. We define the zero-anisotropy hh (lh) energy as $\hbar\omega^0_{hh(lh)}$. Further, we scale our energies by $\hbar\omega^0_{hh}$ to get the diagonal matrix elements for the heavy holes

$$M_{1,1} = M_{4,4} = [(n_x + n_y) + A(n_x - n_y)], \tag{13a}$$

and for light holes,

$$M_{2,2} = M_{3,3} = B + \gamma_n[(n_x + n_y) + A(n_x - n_y)]. \tag{13b}$$

In the Eqs. (13), the anisotropy parameter is defined as

$$A = \frac{\Delta\omega}{\omega_0} = \frac{\omega_x - \omega_y}{\omega_x + \omega_y}, \tag{14}$$

$\gamma_n = \sqrt{(\gamma_1 - \gamma_2)/(\gamma_1 + \gamma_2)}$ characterizes the transverse mass difference. Moreover, we have introduced the hh-lh offset parameter B given by

$$B = \frac{E^z_{lh} + \hbar\omega^0_{lh}}{\hbar\omega^0_{hh}}. \tag{15}$$

The zero of the energy has been chosen so that

$$E^z_{hh} + \hbar\omega^0_{hh} = 0. \tag{16}$$

The parameter B given by Eq. (15), which determines the separation between the lh and hh energy levels, depends on

the ratio of the strength of axial confinement to that of the in-plane confinement as can be seen from the Eqs. (15) and (16), and increase in the value of B reflects enhanced z confinement. Thus, larger values of band-offset parameter correspond to more flattened QDs. The parameter B also facilitates the inclusion of strain in a very simplified manner. The strain in [001]-oriented zinc-blende QD structures changes only the relative position of *lh* and *hh* energy levels without causing any spin mixing.[34,48] This shift in the relative position in SK QDs brought about by strain is found to increase the energy of *hh* relative to *lh*, thus reducing the value of B.[34,49]

The off-diagonal matrix elements calculated using Eqs. (5c) and (5d) in the defined basis [Eq. (7)] are given by

$$M_{1,2} = \sqrt{\frac{3}{2}}\frac{\gamma_3}{(\gamma_1-\gamma_2)^{3/4}}\gamma_n\left\langle\frac{\partial}{\partial z}\right\rangle[\sqrt{1+A}(\sqrt{n_x}\langle n_x',hh|n_x-1,lh\rangle - \sqrt{n_x+1}\langle n_x',hh|n_x+1,lh\rangle)\langle n_y',hh|n_y,lh\rangle - i\sqrt{1-A}(\sqrt{n_y}\langle n_y',hh|n_y-1,lh\rangle - \sqrt{n_y+1}\langle n_y',hh|n_y+1,lh\rangle)\langle n_x',hh|n_x,lh\rangle], \quad (17)$$

and

$$M_{1,3} = \frac{\sqrt{3}}{4}\frac{\gamma_2}{\gamma_1-\gamma_2}\gamma_n\{(1+A)[\sqrt{n_x(n_x-1)}\langle n_x',hh|n_x-2,lh\rangle + \sqrt{(n_x+1)(n_x+2)}\langle n_x',hh|n_x+2,lh\rangle - (2n_x+1)\times\langle n_x',hh|n_x,lh\rangle]\langle n_y',hh|n_y,lh\rangle - (1-A)[\sqrt{n_y(n_y-1)}\times\langle n_y',hh|n_y-2,lh\rangle + \sqrt{(n_y+1)(n_y+2)}\langle n_y',hh|n_y+2,lh\rangle - (2n_y+1)\langle n_y',hh|n_y,lh\rangle]\langle n_x',hh|n_x,lh\rangle - 2i\sqrt{(1+A)(1-A)}[\sqrt{n_x}\langle n_x',hh|n_x-1,lh\rangle - \sqrt{(n_x+1)}\times\langle n_x',hh|n_x+1,lh\rangle][\sqrt{n_y}\langle n_y',hh|n_y-1,lh\rangle - \sqrt{(n_y+1)}\times\langle n_y',hh|n_y+1,lh\rangle]\}, \quad (18)$$

with

$$\langle n_{x(y)}',hh|n_{x(y)},lh\rangle = \int \phi_{n_{x(y)}',hh}(x)\phi_{n_{x(y)},lh}(x)dx. \quad (19)$$

The term $\langle\frac{\partial}{\partial z}\rangle$ in Eq. (17) is given by $\langle\Psi_{m'}(z)|\frac{\partial}{\partial z}|\Psi_m(z)\rangle$ where $\Psi_m(z)$ is the z-dependent part of the wave function and m and m' are the quantum numbers for z confinement.

The scaling that we have chosen implies that the separation between any two distinct *hh* energy levels is unity in the case when $A=0$ and the band mixing is neglected. The anisotropy parameter A can range from -1 to 1, the positive values indicating stronger confinement along the x direction and negative values indicating stronger confinement along y, $A=0$ being the isotropic case. The parameter A can vary from one QD to another in an ensemble of self-assembled QDs and must be fitted to the experimental data for a particular QD. Similarly, the *hh-lh* offset parameter B which represents the strength of axial confinement must be determined for a particular QD from the experiments.

The matrix obtained above can be diagonalized to obtain the energy eigenvalues and eigenfunctions which are used subsequently for the calculation of dipole matrix elements for the interband transitions.

III. DIPOLE MATRIX ELEMENTS

The dipole matrix elements are determined by the selection rules for the Bloch wave functions as well as the envelope functions. The wave functions obtained after diagonalization of the Hamiltonian as outlined in the preceding section can be written as

$$|\psi_n^v\rangle = \sum_{n'} a_{n,n'}\phi^{n'}(x,y)u_{m_j}^v, \quad (20)$$

where $a_{n,n'}$ are the components of the nth eigenvector with $n'=(n_x',n_y',m_j)$ corresponding to the set of quantum numbers characterizing the hole state n'. The dipole matrix element for transition between valence band and conduction band is given by[40]

$$\langle\psi_{n_c}^c|\mathbf{e}\cdot\mathbf{p}|\psi_n^v\rangle = \sum_{n'} a_{n,n'}I_{n',n_c}\langle u_{m_s}^c|\mathbf{e}\cdot\mathbf{p}|u_{m_j}^v\rangle. \quad (21)$$

Here, $\mathbf{e}$ is the direction of polarization, $\mathbf{p}$ is the momentum, and I_{n',n_c} is the overlap integral for the conduction band and valence band envelope functions given by

$$I_{n',n_c} = \int \phi_{n_c}^c(x,y)\phi_{n'}^v(x,y)dxdy \quad (22)$$

with n_c characterizing the state of the conduction electron.

We have considered linearly polarized light making an angle θ with the x axis. This gives the following matrix elements for the Bloch functions:

$$\left\langle\frac{1}{2}\uparrow\middle|\mathbf{e}\cdot\mathbf{p}\middle|\frac{3}{2},\frac{3}{2}\right\rangle = -\frac{1}{\sqrt{2}}\frac{m_0P}{\hbar}ie^{i\theta}, \quad (23)$$

$$\left\langle\frac{1}{2}\downarrow\middle|\mathbf{e}\cdot\mathbf{p}\middle|\frac{3}{2},\frac{1}{2}\right\rangle = -\frac{1}{\sqrt{6}}\frac{m_0P}{\hbar}ie^{i\theta}, \quad (24)$$

$$\left\langle\frac{1}{2}\uparrow\middle|\mathbf{e}\cdot\mathbf{p}\middle|\frac{3}{2},-\frac{1}{2}\right\rangle = \frac{1}{\sqrt{6}}\frac{m_0P}{\hbar}ie^{-i\theta}, \quad (25)$$

and

$$\left\langle\frac{1}{2}\downarrow\middle|\mathbf{e}\cdot\mathbf{p}\middle|\frac{3}{2},-\frac{3}{2}\right\rangle = \frac{1}{\sqrt{2}}\frac{m_0P}{\hbar}ie^{-i\theta}, \quad (26)$$

where P is the Kane matrix element and m_0 is the free electron.

The degree of linear polarization is given by

$$P_{\text{lin}} = \frac{I_{\max}-I_{\min}}{I_{\max}+I_{\min}} \quad (27)$$

with $I_{\max}$ and $I_{\min}$ being the maximum and minimum intensities obtained by varying the angle θ. For a particular transition, the intensity can be obtained from the square of the

absolute value of the corresponding dipole matrix element given by Eq. (21).

IV. RESULTS AND DISCUSSION

In this section, we present detailed numerical analyses of the effect of shape and size anisotropy of CdSe QDs on their optical properties. The material parameters used are effective mass of electron $m_c=0.11m_0$. Luttinger parameters, $\gamma_1=2.1$, $\gamma_2=0.55=\gamma_3$.[44]

Eigenvalues and eigenvectors are obtained on numerically diagonalizing the matrix defined by Eqs. (13)–(19). We have worked with the assumption that the confinement potential along the z direction is stronger as compared to that in the x and y directions for the SK QDs. The stronger confinement in the z direction simplifies the calculation because it allows for the use of the decoupling approximation, whereby the wave function can be separated in the z and the $(x\text{-}y)$ coordinates.[40] Further, this leads to a large energy separation between the adjacent levels arising due to z confinement. Thus one can neglect the coupling between them and consider only the lowest level in terms of z coordinate given by $\Psi_0(z)$, so that the term $\langle \frac{\partial}{\partial z} \rangle$ reduces to $\langle \Psi_0(z) | \frac{\partial}{\partial z} | \Psi_0(z) \rangle$. If we assume that z confinement is symmetric about the $(x\text{-}y)$ plane, leading to definite parity wave functions, then $\langle \frac{\partial}{\partial z} \rangle$ becomes zero from parity considerations.[34] An important consequence of this approximation is that the Hamiltonian has block diagonal form, so that all the energy levels are doubly degenerate. Thus, if one of the eigenstates comprises of the *hh* contribution from $J_z=+3/2$ and *lh* contribution from $J_z=-1/2$, we invariably get another eigenstate with the same energy but the $[+3/2,-1/2]$ components being replaced by $[-3/2,+1/2]$. The total polarization has been calculated by summing over the doubly degenerate states. In the following discussion, we have considered the eigenstates composed of only $+3/2$ and $-1/2$ hole states and we have used the notation $[J_z(n_x,n_y)]$ for depicting our basis states.

In our analysis, we examine the features of energy eigenvalues, wave functions and the degree of linear polarization as a function of the anisotropy parameter A. The energies in all the plots are scaled by a factor of the ground state *hh* energy ($\hbar\omega_{hh}^0$) as discussed in Sec. II. The plots have been taken for *lh*-*hh* band offset parameter $B=0.5$, 1.0, and 1.5. The significance of these values of B can be understood from Figs. 1(a)–1(c) where we have plotted the variation of hole energy eigenvalues for the case when band mixing is neglected. The offset parameter $B=0.5$ corresponds to the situation when at $A=0$, the *lh* ground state lies between the ground state and the first excited state of the *hh*. $B=1.0$ makes the *lh* ground state degenerate with the first excited *hh*, and $B=1.5$ leads to the condition of the first excited *hh* being situated below the ground state of the *lh*. Numerical estimates based on Eq. (15) lead to the result that for all three values of B as taken above, the confinement in the z direction is stronger as compared to that in either of the x or y directions.

It is apparent from Fig. 1 that the hole energies vary linearly with the anisotropy and the variations are large enough to lead to crossing of various excited states. This crossing between various levels depends upon anisotropy A and the value of the offset parameter B.

Although the figures have been plotted for $0.0 \leqslant A \leqslant 1.0$ for the sake of completeness, the results would not be physically meaningful for $A \approx 1$ because it depicts zero confinement along the y direction, i.e., it becomes a quantum wire and would require the corresponding quantum number n_y to take a continuum of values. We have performed calculations considering the maximum value for the quantum numbers n_x or n_y (i.e., $n_{\max}$) to be 5. This gives a matrix of size 144×144. We find that for the states considered in our computations, $n_{\max}=5$ gives the same results as would be obtained for $n_{\max}=6$, for a value of anisotropy $A \leqslant 0.7$. Thus, we have truncated our calculations at $n_{\max}=5$ in the present analysis.

The energy eigenvalues in Figs. 1(d)–1(f) include the effects of band mixing. The mixing can lead to significant change in the energy levels when the band offset is such that it brings the appropriate *lh* and *hh* levels close together. As seen from Figs. 1(a)–1(c), the states which are degenerate in the absence of mixing at zero anisotropy, due to the symmetry of the QD, become nondegenerate on inclusion of band mixing effects. The reason for the removal of degeneracy at zero anisotropy lies in the fact that the orbital angular momentum coming from the envelope wave function is no longer a good quantum number when the full Luttinger Hamiltonian is taken into consideration. Here, the conserved quantity is the total angular momentum **F** which is the sum of the envelope angular momentum (**L**) and the angular momentum of the Bloch part of the wave function (**J**) coming from the Luttinger Hamiltonian. It should also be noted that although total angular momentum **F** is a conserved quantity at zero anisotropy ($A=0$), this is no longer true at a finite value of A.

Further, the valence subband mixing effects manifest in the redshifting of the energy levels as can be seen in Figs. 1(d)–1(f) together with a reduction in the separation between the energy levels as compared to Figs. 1(a)–1(c). The ground state *hh* energies remain almost unaffected by mixing irrespective of the value of B. It is clear from the figures that the intermediate values of anisotropy parameter A cause complex features of crossings of levels or the so-called accidental degeneracies for certain states and avoided crossings for others. A close look at Fig. 1(d) for $B=0.5$ shows a crossing of states S_2 and S_3 at $A=0.47$ and an anticrossing of states S_2 and S_6 for $A=0.72$. Similar features of crossings and anticrossings are obtained for $B=1.0$ [Fig. 1(e)] and $B=1.5$ [Fig. 1(f)]. These features can be understood with the help of the corresponding eigenvector plots. In Fig. 2, we have plotted the squared amplitudes of the components of the eigenvectors for the value of $B=0.5$. We can see that the lowermost level [Fig. 2(a)] is almost a pure *hh* state $[+\frac{3}{2}(0,0)]$, though at higher anisotropy there is a small contribution from the *lh* component $[-\frac{1}{2}(0,0)]$. This is obvious from the fact that there is a large energy separation between the lowest and the first excited state particularly at low anisotropies. As can be seen from Figs. 2(b) and 2(c) the excited states are far from being pure states. Figure 2(b) shows the eigenvector for the first excited state as a function of anisotropy. The state S_2,

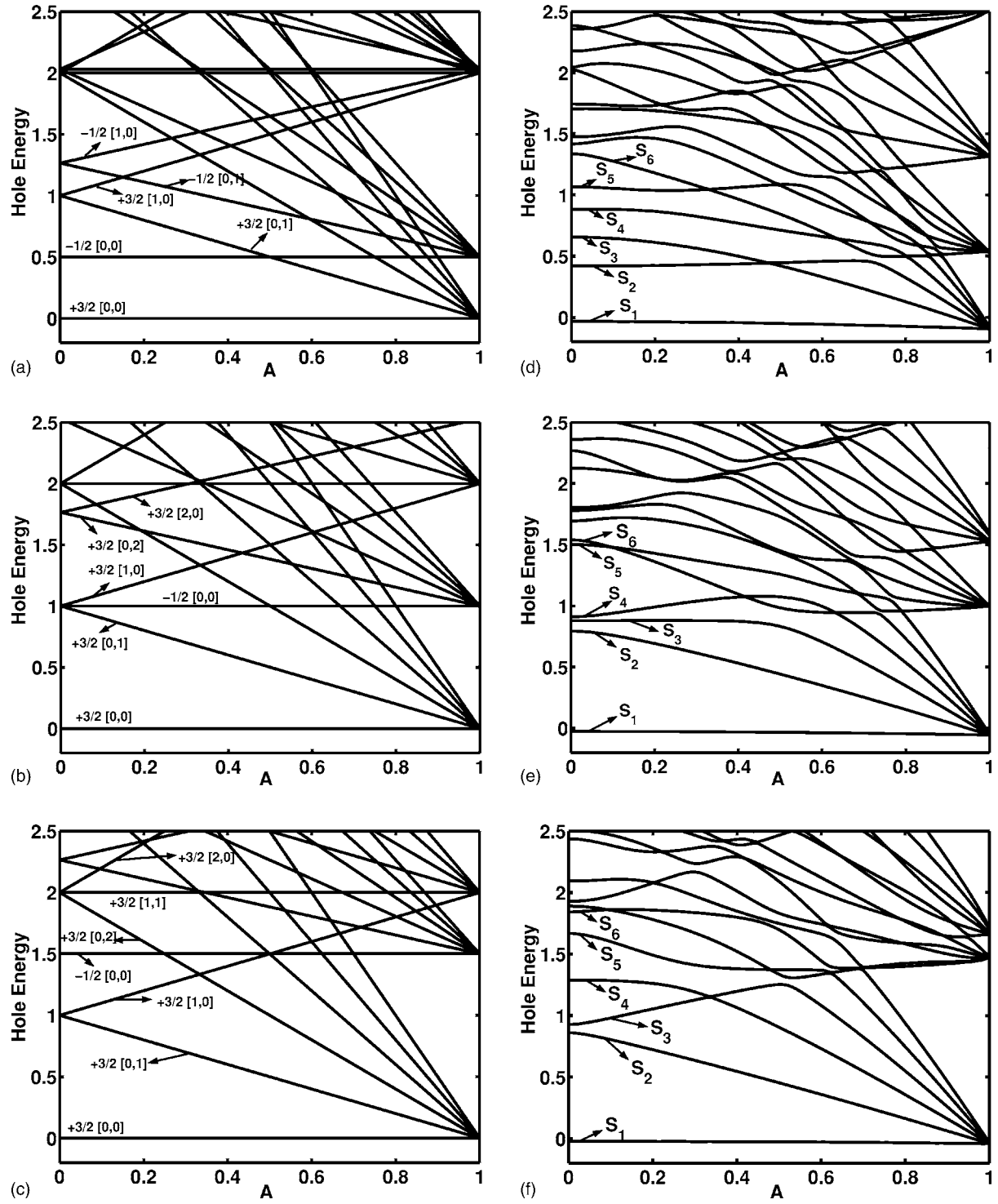

FIG. 1. Variation of hole energy eigenvalues with anisotropy parameter A in CdSe QDs. Plots (a)–(c) correspond to the value of *lh*-*hh* offset parameter $B=0.5$, 1.0, and 1.5, respectively, when the effect of valence subband mixing is neglected. Plots (d)–(f) are the corresponding plots with the inclusion of band mixing effect.

which has ground state *lh* $\left[-\frac{1}{2}(0,0)\right]$ character at low anisotropies, shows strong mixing at an anisotropy of about 0.7, beyond which it switches to almost pure *hh* $\left[+\frac{3}{2}(0,2)\right]$ state. On the other hand, state S_3 shows a significant mixture of *hh* $\{\left[+\frac{3}{2}(0,1)\right], \left[+\frac{3}{2}(1,0)\right]\}$ and *lh* part $\{\left[-\frac{1}{2}(0,1)\right], \left[-\frac{1}{2}(1,0)\right]\}$, but it acquires $\left[+\frac{3}{2}(0,1)\right]$ character predominantly, at intermediate values of A. Further increase in A leads to a small contribution from $\left[-\frac{1}{2}(0,1)\right]$.

The results obtained above can be physically interpreted as follows. All energy states have a definite parity under the two-dimensional inversion defined as $\Pi_{x,y}=(x,y)\rightarrow(-x,-y)$. This is expected in our case because the Hamiltonian re-

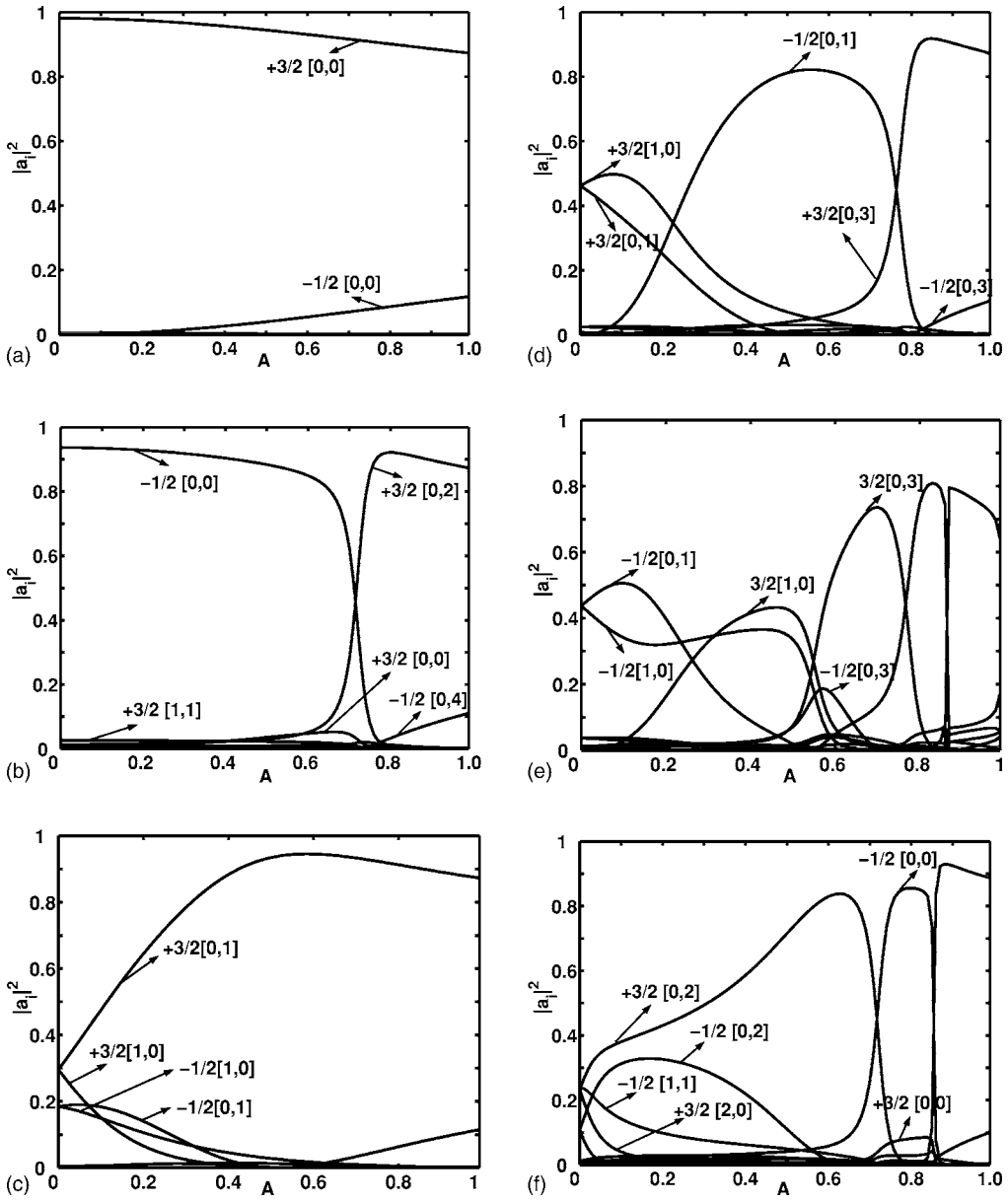

FIG. 2. Components of eigenvectors versus the anisotropy parameter for $B=0.5$ in CdSe QDs. Plots (a)–(f) correspond to the different hole eigenstates S_1-S_6 as labeled in Fig. 1(d).

mains invariant under the above transformation when the term b in Eqs. (4) and (5) is zero. Further, we note that the states with different parity do not interact and thus they show a crossing. However, the states with the same parity show a strong repelling behavior. The term c has even parity under the transformation $\Pi_{x,y}$ and thus, it will couple the states with the same parity while it would vanish for states with opposite parity. The term b which would mix the states with opposite parities is neglected in our analysis so that these states stay uncoupled. Justification for neglecting this term is based on the fact that the term b evaluates to $M_{1,2}$ [Eq. (17)] containing the term $\langle \frac{\partial}{\partial z} \rangle$ which has been taken to be zero.

Figure 3 exhibits the degree of linear polarization for allowed transitions varying with respect to anisotropy A. We have considered transitions from the valence band states to the lowest conduction band state only since the next higher conduction band state is energetically far apart. As discussed earlier, all the states have a definite parity. Since the lowest conduction band state has even parity, only the transitions from even parity valence band states are allowed. These figures show that the degree of linear polarization is zero for all the allowed states at $A=0$. This is because zero anisotropy means a symmetric QD with no preference for a particular orientation of linear polarized light. For the transition from the lowest hole state, the degree of polarization (P_{lin}) shows a monotonic increase with increasing anisotropy. It is interesting to note that the value of offset parameter B also affects the degree of linear polarization. As we can see from Fig. 3(a), the magnitude of P_{lin} gradually decreases with increasing B. This feature can be attributed to the fact that enhancement in B leads to larger energy separation. As a consequence, the mixing between the different contributing states

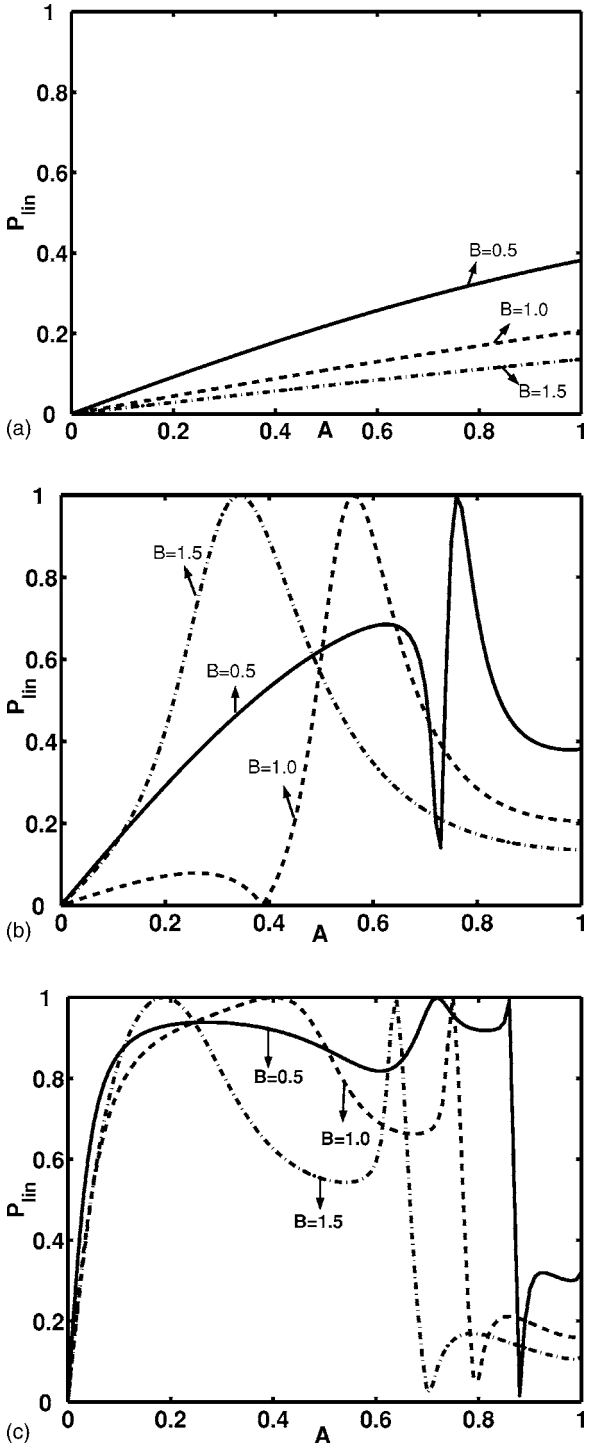

FIG. 3. Degree of linear polarization as a function of the anisotropy parameter for the allowed transitions, for different values of offset parameter B in CdSe QDs. Plot (a) corresponds to the lowest allowed transitions from state S_1 for all three values of B; plot (b) is for the next allowed excited states S_2, S_3, S_4 corresponding to the B values 0.5, 1.0, and 1.5, respectively; and plot (c) is for the states S_6, S_6, S_5, the next higher allowed states at $B=0.5, 1.0, 1.5$, respectively. The states are as labeled in Figs. 1(d)–1(f).

is reduced which is manifested in Fig. 2(a) as well. It is well known that transitions from pure *hh* or *lh* states lead to circularly polarized emission and/or absorption, whereas, linear polarized output can be obtained from states with an admixture of *hh* and *lh* states.[12,50] Thus, if the coupling between the different *hh* and *lh* states weakens, the degree of linear polarization decreases. For higher energy states, we find that P_{lin} does not exhibit linear variation with anisotropy but a complex plot is obtained. As seen in the Fig. 3(b), the next excited state shows a peculiar behavior when anisotropy is changed. For the curve at $B=0.5$, a gradual increase of P_{lin} can be seen for $A \leqslant 0.6$, beyond which there is a steep fall in the magnitude of P_{lin}. The features for higher values of B are qualitatively similar to the case of $B=0.5$ although the peak shifts towards lower values of A with increase in B. In addition, the peaks become sharper and clearly distinguishable for higher states with increasing B, which physically implies that polarization resolved PL spectrum of larger QDs is more sensitive to shape anisotropy which conforms with experimental results.[15]

The features of the polarization curves can be explained on the basis of corresponding eigenvector plot in Fig. 2. At the values of anisotropy parameter A where the states exhibit strong mixing behavior, we can see sharp peaks in the graphs for P_{lin}. But a careful examination reveals a slight change in corresponding values of A in the polarization and eigenvector curves. This feature may be ascribed to the fact that the calculation of P_{lin} involves multiplication of eigenvectors with the weight factors, i.e., the overlap integral between conduction and valence band basis functions, and the interband matrix element given by Eqs. (20)–(23). For low values of A, the major contribution is from states $\left[-\frac{1}{2}(0,0)\right]$ and $\left[+\frac{3}{2}(0,0)\right]$. With increasing anisotropy, the coupling between these two states increases, leading to the initial increase in the degree of polarization. Though the contribution of the $\left[+\frac{3}{2}(1,1)\right]$ state appears negligible in the plot, with the inclusion of the weight factors it becomes significant. The magnitude of P_{lin} shows a sharp fall at $A \sim 0.65$. This can be understood from the fact that around this order of anisotropy, $\left[+\frac{3}{2}(0,0)\right]$ and $\left[-\frac{1}{2}(0,0)\right]$ states have very small contributions. With further increase in anisotropy, we see an abrupt rise in the magnitude of P_{lin}. The abnormal behavior essentially has its origin in the fact that the $\left[+\frac{3}{2}(0,0)\right]$ and $\left[-\frac{1}{2}(0,0)\right]$ states cross at this point, i.e., there is a strong mixing of the two states.

On the basis of our theoretical model, we have made an attempt to explain some of the experimental results on the degree of polarization in CdSe QDs. Koudinov *et al.*[12] have obtained the PL signal as a function of the polarization analyzer angle for the three quantum dots, viz., QD1, QD2 and QD3. We have tried to plot the same features theoretically as shown in Fig. 4. These figures exhibit the variation of normalized intensity as a function of the angle $\theta' = \theta - \theta_s$ for the values of parameters A, B, and θ_s which provide best fit with the experimental data for QD1 and QD2 of Ref. 12. We have introduced the angle θ_s to account for the fact that there is an angular shift in the theoretical curves as compared to the experimental ones, which can be attributed to the fact that the orientation of QDs is random and the PL intensity depends on the QD orientation. Figure 4(a) is plotted at $B=0.1$ and $A=0.18$ and Fig. 4(b) is for $B=0.2$ and $A=0.26$. It is clear that our theoretical fits are qualitatively in good

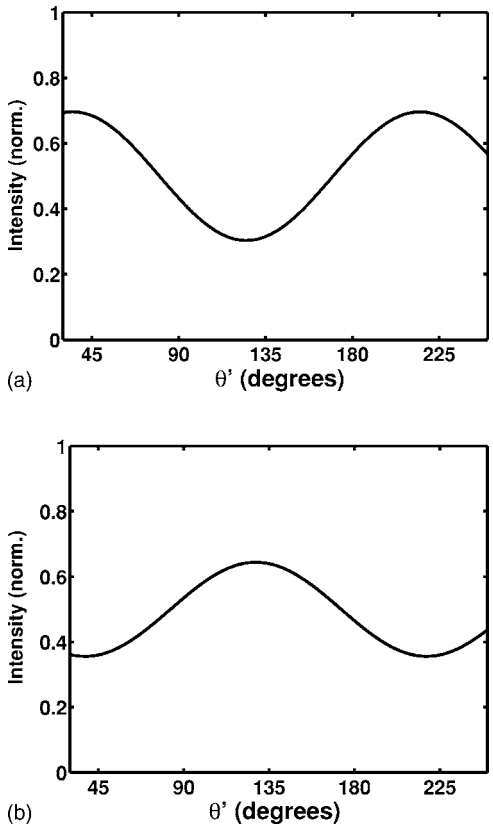

FIG. 4. Normalized intensity as a function of angle (θ') for different values of A and B in CdSe QDs. The values of the parameters chosen are (a) $A=0.18$, $B=0.1$, $\theta_s=55°$ and (b) $A=0.26$, $B=0.2$, $\theta_s=142°$.

agreement with the experimental observations of Koudinov *et al.*[12] We have calculated the angular shift θ_s for the above two cases which turns out to be 55° for QD1 and 142° for QD2, which indicates that QD1 is oriented at an angle of 10° with respect to [110] while QD2 is oriented at an angle of 7° with $[1\bar{1}0]$ direction. QD3 which shows very small degree of polarization is likely to be an isotropic quantum dot.

Kiessling *et al.* have reported the degree of linear polarization for CdSe QD ensemble to vary between 25%–28% which can be obtained by taking the value of $B=0.2$ and A ranging between 0.24 and 0.25 in our numerical calculations. Thus, we find that the high values of the degree of polarization of the lowest-state PL intensity can be obtained if the *hh* and *lh* states have small energy separation corresponding to small values of B or the QD is highly anisotropic, i.e., A is large. A unique set of B and A values can be arrived at, only if the results of polarization resolved PL/PLE experiments are considered for a number of excited states over a set of QDs.

V. CONCLUSIONS

We have examined the effect of structural anisotropy of quantum dots on the hole energy levels, wave function and degree of linear polarization of the PL spectra. The excited states are found to be more sensitive to anisotropy while the ground states are relatively less affected. We find prominent effect of valence subband mixing even for isotropic quantum dots, but the effects get significantly pronounced for anisotropic dots. The degree of linear polarization depends strongly on anisotropy with its value reaching close to unity for a specific range of anisotropy parameter. The variation of degree of polarization is not monotonic with anisotropy which appears to be the reason why experimental studies could not obtain a correlation between the optical and geometrical anisotropy.[11] The numerical estimates made for CdSe QDs grown by SK method show a reasonable degree of qualitative agreement with the experimental results reported very recently.

ACKNOWLEDGMENTS

The authors express their sincere gratitude to F. Henneberger, Institut für Physik, Humboldt Universität zu Berlin for his critical comments as well as valuable suggestions throughout the work. The authors are indebted to P. Sen, J. Puls, I. Akimov, and A. Hundt for insightful discussions. The authors gratefully acknowledge the financial support from DST, India and DAAD, Germany under the DST-DAAD program. One of the authors (S.K.) is thankful to DST, India for providing financial assistance. One of the authors (S.K.G.) is grateful to the Council for Scientific and Industrial Research.

*Electronic address: prakusen@rediffmail.com

[1] V. Zwiller, L. Jarlskog, M.-E. Pistol, C. Pryor, P. Castrillo, W. Seifert, and L. Samuelson, Phys. Rev. B **63**, 233301 (2001).
[2] I. A. Akimov, K. V. Kavokin, A. Hundt, and F. Henneberger, Phys. Rev. B **71**, 075326 (2005).
[3] T. Flissikowski, I. A. Akimov, A. Hundt, and F. Henneberger, Phys. Rev. B **68**, 161309(R) (2003).
[4] C. S. Kim *et al.*, Phys. Rev. Lett. **85**, 1124 (2000).
[5] S. Lee, I. Daruka, C. S. Kim, A.-L. Barabási, J. L. Merz, and J. K. Furdyna, Phys. Rev. Lett. **81**, 3479 (1998).
[6] F. Gindele, U. Woggon, W. Langbein, J. M. Hvam, K. Leonardi, D. Hommel, and H. Selke, Phys. Rev. B **60**, 8773 (1999).
[7] F. Meier and D. D. Awschalom, Phys. Rev. B **71**, 205315 (2005).
[8] J. Brault, M. Gendry, G. Grenet, G. Hollinger, J. Olivares, B. Salem, T. Benyattou, and G. Bremond, J. Appl. Phys. **92**, 506 (2002).
[9] G. V. Astakhov, T. Kiessling, A. V. Platonov, T. Slobodskyy, S. Mahapatra, W. Ossau, G. Schmidt, K. Brunner, and L. W. Molenkamp, Phys. Rev. Lett. **96**, 027402 (2006).
[10] T. Kiessling, G. V. Astakhov, A. V. Platonov, T. Slobodskyy, S. Mahapatra, W. Ossau, G. Schmidt, K. Brunner, and L. Molenkamp, Phys. Status Solidi C **3**, 912 (2006).

[11] I. Favero, G. Cassabois, D. Darson, C. Voisin, C. Delalande, P. Roussignol, and J. M. Gérard, Physica E (Amsterdam) **26**, 51 (2005).
[12] A. V. Koudinov, I. A. Akimov, Y. G. Kusrayev, and F. Henneberger, Phys. Rev. B **70**, 241305(R) (2004).
[13] Y. G. Kusrayev, A. V. Koudinov, B. P. Zakharchenya, S. Lee, J. K. Furdyna, and M. Dobrowolska, Phys. Rev. B **72**, 155301 (2005).
[14] F. A. Zhao, J. Wu, P. Jin, B. Xu, Z. G. Wang, and C. L. Zhang, Physica E (Amsterdam) **23**, 31 (2004).
[15] M. Sugisaki, H. W. Ren, S. V. Nair, K. Nishi, S. Sugou, T. Okuno, and Y. Masumoto, Phys. Rev. B **59**, R5300 (1999).
[16] P. S. Drouvelis, P. Schmelcher, and F. K. Diakonos, Phys. Rev. B **69**, 035333 (2004).
[17] J. J. Finley, D. J. Mowbray, M. S. Skolnick, A. D. Ashmore, C. Baker, A. F. G. Monte, and M. Hopkinson, Phys. Rev. B **66**, 153316 (2002).
[18] I. Favero, G. Cassabois, C. Voisin, C. Delalande, P. Roussignol, R. Ferreira, C. Couteau, J. P. Poizat, and J. M. Gerard, Phys. Rev. B **71**, 233304 (2005).
[19] Y. Z. Hu, M. Lindberg, and S. W. Koch, Phys. Rev. B **42**, 1713 (1990).
[20] L. M. Woods, T. L. Reinecke, and R. Kotlyar, Phys. Rev. B **69**, 125330 (2004).
[21] A. Wojs and P. Hawrylak, Phys. Rev. B **53**, 10841 (1996).
[22] A. H. Rodriguez, C. Trallero-Giner, S. E. Ulloa, and J. Marin-Antuña, Phys. Rev. B **63**, 125319 (2001).
[23] C. E. Pryor and M. E. Flatté, Phys. Rev. Lett. **91**, 257901 (2003).
[24] G. Cantele, G. Piacente, D. Ninno, and G. Iadonisi, Phys. Rev. B **66**, 113308 (2002).
[25] E. Räsänen, A. Harju, M. J. Puska, and R. M. Nieminen, Phys. Rev. B **69**, 165309 (2004).
[26] C. Pryor, M.-E. Pistol, and L. Samuelson, Phys. Rev. B **56**, 10404 (1997).
[27] T. Darnhofer, D. A. Broido, and U. Rössler, Phys. Rev. B **50**, 15412 (1994).
[28] M. Bayer, O. Stern, P. Hawrylak, S. Fafard, and A. Forchel, Nature (London) **405**, 923 (2000).
[29] S. Raymond *et al.*, Phys. Rev. Lett. **92**, 187402 (2004).
[30] A. V. Madhav and T. Chakraborty, Phys. Rev. B **49**, 8163 (1994).
[31] S. H. Wei and S. B. Zhang, Phys. Rev. B **62**, 6944 (2000).
[32] H. H. von Grünberg, Phys. Rev. B **55**, 2293 (1997).
[33] A. D. Andreev, J. R. Downes, D. A. Faux, and E. P. O'Reilly, J. Appl. Phys. **86**, 297 (1999).
[34] C. Lü, J. L. Cheng, and M. W. Wu, Phys. Rev. B **71**, 075308 (2005).
[35] M. Grundmann, O. Stier, and D. Bimberg, Phys. Rev. B **52**, 11969 (1995).
[36] S. Kapoor, J. Kumar, and P. K. Sen, J. Appl. Phys. **95**, 4833 (2004).
[37] S. Kapoor, J. Kumar, and P. K. Sen, Phys. Status Solidi B **242**, 1650 (2005).
[38] J. Planelles, J. Dìaz, J. Climente, and W. Jaskòlski, Phys. Rev. B **65**, 245302 (2002).
[39] J. M. Luttinger and W. Kohn, Phys. Rev. **97**, 869 (1955).
[40] U. Bockelmann and G. Bastard, Phys. Rev. B **45**, 1688 (1992).
[41] W. W. Chow, S. W. Koch, and M. Sargent III, *Semiconductor Laser Physics* (Springer-Verlag, Berlin, 1994), pp. 463–464.
[42] J. H. Davies, *The Physics of Low Dimensional Semiconducors: An Introduction* (Cambridge University Press, Cambridge, 1998).
[43] U. E. H. Laheld and G. T. Einevoll, Phys. Rev. B **55**, 5184 (1997).
[44] A. I. Ekimov, F. Hache, M. C. Schanne-Klein, D. Ricard, C. Flytzanis, I. A. Kudryavtsev, T. V. Yazeva, A. V. Rodina, and A. L. Efros, J. Opt. Soc. Am. B **10**, 100 (1993).
[45] D. J. Norris, A. Sacra, C. B. Murray, and M. G. Bawendi, Phys. Rev. Lett. **72**, 2612 (1994).
[46] V. A. Fonoberov, E. P. Pokatilov, and A. A. Balandin, Phys. Rev. B **66**, 085310 (2002).
[47] J. M. Luttinger, Phys. Rev. **102**, 1030 (1956).
[48] H. J. Lozykowski and V. K. Shastri, J. Appl. Phys. **69**, 3235 (1991).
[49] L. He, G. Bester, and A. Zunger, Phys. Rev. B **70**, 235316 (2004).
[50] L. Besombes, K. Kheng, and D. Martrou, Phys. Rev. Lett. **85**, 425 (2000).